Spatial-temporal evolution analysis and deep learning inversion of water-carbon-three-dimensional ecological footprint of urban agglomeration in the middle reaches of the Yangtze River

Aili Wang[a], Shunsheng Wang[a,b],*, Tengfei Liu[a], Jinyue Yang[a], Ruijie Yang[a]

[a]*School of Water Conservancy, North China University of Water Resources and Electric Power, Zhengzhou 450046, China,
email: wangshunsheng609@163.com (S. Wang)*
[b]*Collaborative Innovation Center for Efficient Utilization of Water Resources, Zhengzhou 450046, China*

ABSTRACT

The urban agglomeration in the Yangtze River's middle reaches is a crucial location of China's economic expansion. Urbanization construction is an important measure to improve human life style, encourage economic and social growth, and improve the level of science and technology. These changes have an impact on the natural environment at the same moment. This research did a detailed investigation on the correlation ecological footprint elements and the construction of three-dimensional ecological footprint model to explore the law of water carbon three-dimensional ecological footprint evolution and its depth-to-breadth learning inversion leads to the growth of cities in the middle reaches of the Yangtze River. The findings indicate that when promoting the process of urbanization, various human activities have a non-negligible impact on the ecological environment. We must pay close attention to environmental challenges as urbanization progresses since both the rise in people's quality of life and the pace of urbanization would result in a continual growth in ecological footprint. And take scientific and effective measures for different problems to make sure the environment and urbanization are developed sustainably.

Keywords: The Yangtze River's middle reaches; Urban agglomeration; Three-dimensional ecological footprint; Temporal and spatial evolution; Deep learning

1. Introduction

The urban agglomeration along the Yangtze River's middle reaches are now experiencing a development boom related to urbanization. The degree of economic growth is rising, but there are a number of ecological and environmental issues that must be addressed [1]. On the urban enclave in the Yangtze River's middle reaches, the level of population urbanization does not match the development of land urbanization, resulting in low land utilization, and changes in land cover affect the food security of cultivated land [2]. The entire ecological environment in the middle reaches of the Yangtze River, where the urban agglomeration is located, is at a high-risk stage. The consumption of ecological energy is increasing day by day, so it is imperative to save energy and reduce emissions to reduce the region's changing ecological imprint [3]. The ecological environment is used at fairly different rates in various geographic scales. Population agglomeration occurs in areas with relatively developed economies, but not in areas with low levels of economic progress. Therefore, the ecological utilization rate of human beings does not match bearing capacity of the environment's ecosystem [4]. Although a large number of agricultural transfer populations migrated to cities, they could not really integrate into cities quickly. Therefore, the middle reaches of the Yangtze River's urban agglomeration's

* Corresponding author.

quality of urbanization development needs to be improved urgently [5]. To address the urban agglomeration's ecological and environmental challenges in the middle sections of the Yangtze River and raise its ecological development level, this study introduces a deep learning model to thoroughly analyze the essential growth of the urban agglomeration along the Yangtze River's middle reaches, the influencing factors of the ecological footprint, and their space-time evolution laws.

2. Related work

A popular intelligence algorithm is deep learning. Modern information science has quickly advanced to the point that it may contribute significantly to many different scientific domains. Some scholars have used deep learning models in conjunction with relevant ecological themes to produce specific study findings. Pichler et al. [6] and other researchers will use various deep learning algorithms to predict biological species in the ecosystem. Algorithms make predictions about the ability of species to interact based on traits, while also inferring combinations of traits that lead to causal relationships between them. Experimental results show that deep learning algorithms have significant advantages in understanding interaction networks, thus verifying the great potential of artificial intelligence such as deep learning in ecological reasoning. Scholars such as Hosu et al. [7] proposed a new deep learning model of KonCept512 to effectively recognize ecological images. In addition, they constructed the KonIQ-10k dataset, which contains 10,073 ecologically valid in-the-wild high-quality scoring images. The proposed model shows excellent resolution and good recognition performance on this dataset. Huang et al. [8] found that traditional machine learning algorithms have limited predictive performance for landslide susceptibility, and then proposed a fully connected backup autoencoder algorithm based on deep learning, namely the FC-SAE model. The model consists of four steps: original feature loss, sparse feature encoder, categorization prediction and sparse feature extraction. The experiment included 23195 landslide grid cells and non-landslide grid cells. The results show that the prediction accuracy of FC-SAE is 81.56%, which is higher than the traditional machine learning model. Researchers such as Barzegar et al. [9] started from water quality monitoring in the ecological environment, combined the LSTM network and CNN network in deep learning, and proposed a CNN-LSTM model. The experiment uses this model to predict factors affecting water quality. The findings suggest that the CNN-LSTM model may assist staff in effectively capturing the change level of water quality factors, confirming deep learning's promising application possibilities in the ecological sector.

A metric for gauging human demand for resources and ecological services is the ecological footprint. Numerous academics have studied the issue of the three-dimensional ecological footprint of urban agglomerations. Taking the Pearl River Delta in China as an example, researchers such as Li et al. [10] developed a three-dimensional footprint model that incorporates the ecological footprint, carbon footprint, and water footprint. On this basis, the problem that the traditional three-dimensional footprint model is still in

a two-dimensional plane under ecological surplus can be improved, and the supply and demand relationship between human and natural capital can be accurately predicted. The results of the study showed that the extent of one's ecological imprint and one's carbon footprint contributed the most to the increase of REP in the study area, and also verified the practicability of the three-dimensional footprint model. Chen et al. [11] proposed a carbon footprint index based on water-carbon-ecological footprint, and took the Central China Triangle as an example to identify its balance between ecological compensation and regional growth. In the experiment, the assessment framework included the Gini coefficient, and other factors were used to evaluate the fairness. The research results fully reflect the practical significance of the three-dimensional model, and can offer a theoretical framework for the long-term growth of TOCC. Scholars such as Lee et al. [12] conducted research on the physical vulnerability of organisms in Taiwan Province. The experiment examines the link between the ecological footprint of rural regions in Taipei and Taiwan and their overall vulnerability using an overlapped methodology. By analyzing the link between ecological footprint and overall vulnerability, the study divides Taipei and rural areas into four types of risk areas. Therefore, local governments can formulate different competitive strategies based on these empirical results, which shows that the ecological footprint analysis method has strong practical significance. To assist in resolving fresh issues threatening China's sustainable development, Wang et al. [13] and other researchers explored the driving forces of natural capital demand. The experiment analyzes the link between domestic economic growth and environmental conservation by using the three-dimensional ecological footprint model and discovers a strong inverted U-shaped association between Economic output and natural resources. Therefore, when the relevant governments allocate natural capital, they need to formulate differentiated environmental policies according to different environments, and at the same time need to improve advance size, technology and structure to improve energy efficiency. The study's findings demonstrate the three-dimensional ecological footprint model's applicability.

To sum up, the three-dimensional ecological footprint of urban agglomerations has strong credibility and practicability, and is a hot topic among researchers. At the same time, deep learning, as an intelligent algorithm, enables researchers to more clearly and extensively examine the influencing variables of ecological footprint. As a result, to address the ecological environment challenges of the urban agglomeration in the Yangtze River's middle reaches, this experiment introduced a deep learning model to discuss the fundamental growth of the urban agglomeration in the Yangtze River's middle reaches, the variables impacting the ecological footprint, and its temporal and geographical history.

3. Analysis of influencing factors of ecological footprint and its temporal and spatial evolution

3.1. Correlation influencing factors of ecological footprint

Ecological footprint is a kind of development index, which is used to study human production activities and

ecological environment. The ecological footprint examines in depth how the size of the land area affects human consumption and the effects of such activities on the ecosystem. This area refers to the needed amount of land for generating resources needed by human beings and disposing the wastes caused by these resources [14,15]. According to the applicable theory of ecological footprint, there are six different categories of productive land that are affected by human production and production activities: agricultural land, grassland, woodland, water, construction land, and land used for fossil fuels [16]. The ecological footprint is often affected by many aspects, and it is closely related to the spatial effect and urbanization process, as shown in Fig. 1.

The aforementioned figure demonstrates that the effects of urbanization on the environment cannot be ignored, and there is a two-way interaction between various human production and living activities and the ecological environment system. Urbanization-related factors such as population growth, land urbanization changes, changes in energy factors, economic development, scientific and technological advancements, and improvements in industrial structure all interact with one another and have a big impact on how the ecological footprint evolves [17]. This effect is two-sided, one is promoting, the other is inhibiting. This effect promotes changes in the size of the footprint, the functional structure of the footprint, and the ecological footprint's historical development, which in turn makes the evolution of the ecological footprint counteract the urbanization process [18]. In addition, spatial effects also affect the evolution of the environmental impact to some degree, so I will not repeat them here. The seven stages of urbanization are the major influencing elements, and Fig. 2 illustrates how population urbanization has affected the development of ecological footprint.

According to Fig. 2, it is clear that the relationship between population urbanization and the growth of the ecological footprint primarily involves four components: changing people's lifestyles, increasing population density, raising people's levels of education, and improving population quality. The development of population urbanization

has improved per capita income to a certain extent, and its living needs have been met. However, the growth and diversification of consumption followed, which caused ongoing use of ecological and environmental resources, which eventually led to the increase in ecological footprint and the decline in the per-person ecological environment's carrying capacity. The continual growth of culture, on the other hand, which greatly raises population quality, is the beneficial consequence of population urbanization. Therefore, environmental protection technologies and policies have been innovated and implemented, which can effectively reduce the strain on the natural environment. The effects of modernizing industrial structures on the development of ecological footprint can be expressed as an Environmental Kuznets Curve, as shown in Fig. 3.

Urbanization may be broken down into three phases. The ecological footprint is tiny, the abundance of ecological resources is great, and human use of ecological resources is minimal in the first stage, which is dominated by the primary industry. In the second stage based on industrial development, the utilization rate of land resources has been significantly enhanced, carbon emissions have continued to increase, the consumption of ecological environmental resources has also continued to increase, and the scale of ecological footprint has expanded significantly. Early in the third stage and in the late stages of the second stage, technology and scientific advancement, the elevation of population standards, and modifying the industrial structure have
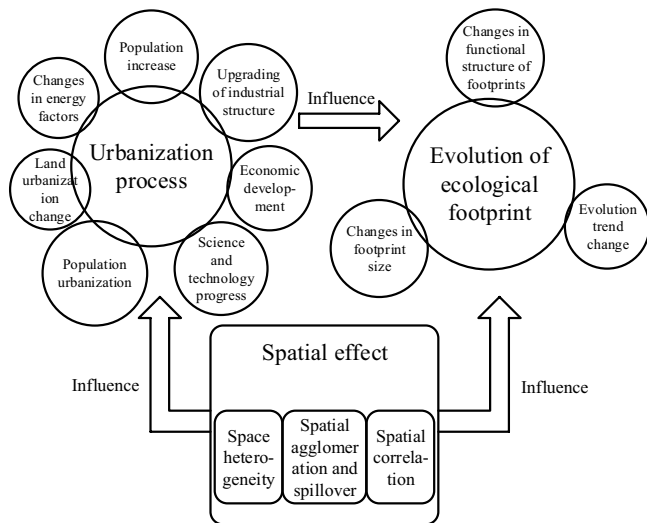

Fig. 2. Impact of population urbanization on the evolution of ecological footprint.

Fig. 1. Relationship among spatial effect, urbanization process and ecological footprint evolution.

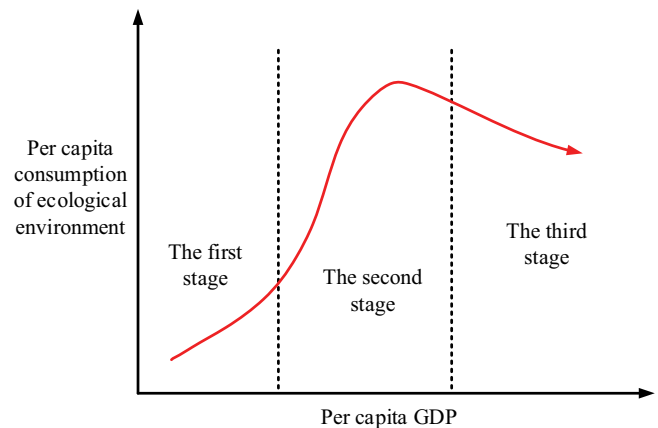Fig. 3. Environmental Kuznets curve changes in the process of urbanization.

effectively controlled the consumption of ecological environmental resources, and the ecological footprint's size has decreased over time.

3.2. Model construction and temporal and spatial evolution analysis of 3D ecological footprint

Environmental carrying capacity and ecological deficiency serve as the primary markers of the ecological footprint. The former is the total of the ecologically productive land area that may be delivered to humans in a given location to demonstrate the ecosystem's resource supply capability in that area [19]. Since the land productivity in various locations must vary, it is required to standardize the ecological carrying capacity calculation in dimensions to guarantee the comparability and summing of the carrying capacity is accurate. The calculation formula is shown in Eq. (1):

$$BC = \frac{\sum_{i}^{n} A_i \times q_i \times y_i}{N} \tag{1}$$

where BC denotes the region's per capita ecological carrying capacity, N represents the total population of the area, A_i represents the whole surface area of Class i land in the area, q_i and y_i reflect the equilibrium and yield factors of Class i land, respectively. The ecological deficit is the difference between an area's ecological footprint and its ecological carrying capability, which is used to demonstrate that the ecological demand of the area has surpassed the bearing capacity and supply capacity of the ecological environment [20]. The three-dimensional ecological footprint model is built on the two-dimensional model, which organically integrates the width and depth of the ecological footprint, so the three-dimensional ecological footprint model may be stated mathematically in Eq. (2).

$$EF = BC + ED = EF_{size} \times EF_{depth} \tag{2}$$

where EF represents the environmental footprint, BC is still the carrying capacity of the environment, and ED is the ecological deficit, EF_{size} and EF_{depth} represents the breadth and depth of the ecological footprint, respectively. The schematic representation of the ecological model's translation from 2D to 3D is shown below.

Fig. 4 clearly shows that the standard two-dimensional ecological model is made up of two concentric rings. The inner circle represe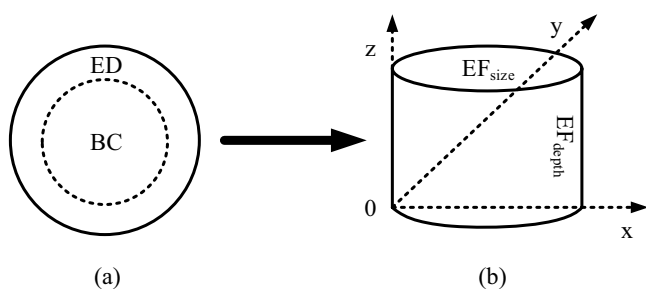nts ecological carrying capacity, whereas the outside circle represents ecological deficiency. The overall model is shown in Fig. 4a. After adding the ecological footprint, a 3D ecological model was generated. The 3D ecological model is generated by multiplying the footprint width and footprint depth, as demonstrated by the cylinder in Fig. 4b. The actual area of ecologically productive land inhabited within the permissible range of ecological carrying capacity is referred to as footprint width. It can completely present the occupation and level of all flow capital, and the specific calculation formula is shown in Eq. (3).

$$EF_{size} = \frac{EF}{EF_{depth}} \qquad \left(0 < EF_{size} \leq BC\right) \tag{3}$$

In Eq. (3), it is clear that the calculation of footprint width is closely related to footprint depth. The footprint depth represents the bottom surface in the three-dimensional ecological model, and the deep meaning is the land area under the consumption level of environmental resources in the area, which can be calculated by Eq. (4).

$$EF_{depth} = 1 + \frac{ED}{BC} \tag{4}$$

Eq. (4) demonstrates that while calculating the footprint depth, both ecological deficit and ecological carrying capacity are required, and that the combination of the two can properly calculate the footprint depth and then reveal the degree of stock capital consumption. It should be mentioned that, usually in the basic three-dimensional ecological model, the differences in nature between ecological deficit and ecological surplus are often easily confused. Therefore, the footprint depth is too low and the footprint width is too high [12]. When there is a difference between particular locations that causes the basic model to be limited, it is required to enhance the linked algorithms of footprint width and footprint depth, as shown by Eqs. (5) and (6), respectively.

$$EF_{depth,region} = 1 + \frac{\sum_{i=1}^{n} \max\{EF_i - BC_i, 0\}}{\sum_{i=1}^{n} BC_i} \tag{5}$$

$$EF_{size,region} = \sum_{i=1}^{n} \min\{EF_i, BC_i\} \tag{6}$$

where i represents a total of six kinds of environmentally beneficial land: cultivated land, grassland, forest land, water area, land for development and land for fossil energy. EF_i denotes the ecological footprint contained in the i site; BC_i refers to the area's ecological carrying capacity; $EF_{depth,region}$ and $EF_{size,region}$ indicates the depth and breadth of the regional footprint, respectively. Based on this, Eq. (7) can be obtained.

Fig. 4. Schematic diagram of converting two-dimensional ecological model into three-dimensional ecological model.

$$
\begin{aligned}
EF_{3D,region} &= EF_{size,region} \times EF_{depth,region} \\
&= \sum_{i=1}^{n} \min\{EF_i, BC_i\} \times \left(1 + \frac{\sum_{i=1}^{n} \max\{EF_i - BC_i, 0\}}{\sum_{i=1}^{n} BC_i}\right)
\end{aligned} \tag{7}
$$

Eq. (7) depicts the three-dimensional ecological footprint calculation algorithm from a regional scale viewpoint.

4. Effects of urban agglomeration on ecological footprint in the middle reaches of the Yangtze River based on deep learning

4.1. Model construction and training process of deep learning inversion

The deep learning model has a hierarchical structure that is quite similar to the normal neural network model. Both model systems are made up of three layers: the input layer, the hidden layer, and the output layer. It should be noted that the nodes between two neighboring levels are completely linked, that is, when nodes in the same layer or cross-layer nodes are connected, each layer may be treated as a logistic regression model [21]. Fig. 5 depicts the deep learning model's structure.

According to Fig. 5, three hidden layers are incorporated in deep learning's multi-layer structure. The network will perform poorly in terms of training efficiency and underfitting if all structural layers are trained simultaneously. On the other hand, to get rid of various problems in traditional models, deep learning models apply innovative training mechanisms. This innovative training mechanism works well. First, a single layer of neurons is constructed in sequence according to the order of the structural layers, and each time the network is trained, its object is a single structural layer. After the network training of all structural layers is completed, relevant algorithms are applied to optimize it. Prior to refinement, all structural layer parameters must be obtained in an unsupervised way. Next, network training must be carried out layer by layer from the bottom to the top, or feature extraction. Then, the supervised reverse learning method is applied to optimize the parameters of all structural layers, that is, the mistake is from top to bottom reversed. The indispensable process in deep learning is sparse auto-encoding, and its operating mechanism is shown in Fig. 6.

The deep learning auto-encoding model and the conventional neural network model's workings are contrasted in Fig. 6a. On the left is the fo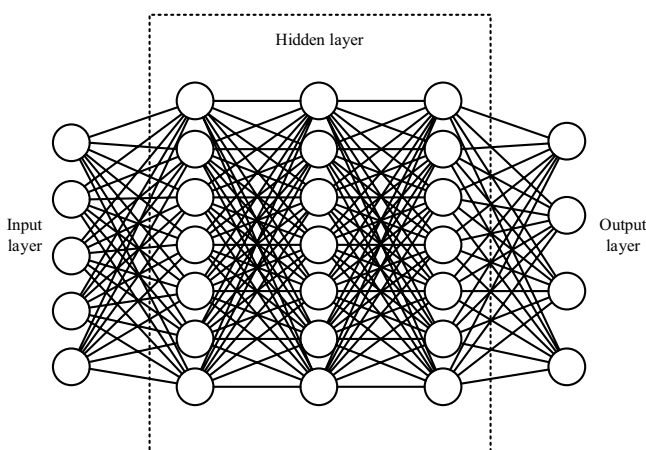rmer, each input sample carries a specific label, transmits data with very little information, and adjusts all parameters. The latter is on the right, by using the corresponding encoding algorithm to perform feature extraction and encoding operations on all information data without labels. The use of the tuning mechanism in the deep learning autoencoder is shown in action in Fig. 6b. After the automatic encoder completes the encoding, all input data will be correspondingly encoded, and the reverse decoder can be applied to reconstruct it to obtain the restored data information. The quality of the encoder is then assessed by comparing the initial information with the recovered reconstruction data information. If the $L1$-norm on the automatic encoder has a regularization constraint, the encoder is converted to a sparse encoder, and its input calculation formula is shown in Eq. (8).

$$h = W^T X \tag{8}$$

From Eq. (8), it is evident that at this time, only a small number of nodes in each layer are not zero, and the formula representing the network training loss is shown in Eq. (9).

$$L(X;W) = \|Wh - X\|^2 + \lambda \sum_j |h_i| \tag{9}$$

Sparse coding is a learning algorithm with an unsupervised approach at its core. The appropriate parameter values, basis vectors, and crucial coefficients can be eventually solved by a sequence of optimization and reconstruction.

4.2. Inversion analysis of surface wave dispersion curve from the perspective of deep learning

When surface wave dispersion curves are inverted, effectively extracting the observed dispersion curves is first required. On this basis, after calculating the theoretical dispersion curve using the given density ϱ, layer thickness h, shear wave velocity V_s, and longitudinal wave velocity V_p and other related data, the mean square error of the two dispersion curves is defined as shown in Eq. (10) Invert the objective function:

$$E = \sqrt{\frac{1}{N}\sum_{i=1}^{N}\left(Vr_i^{obs} - Vr_i^{cal}\right)^2} \tag{10}$$

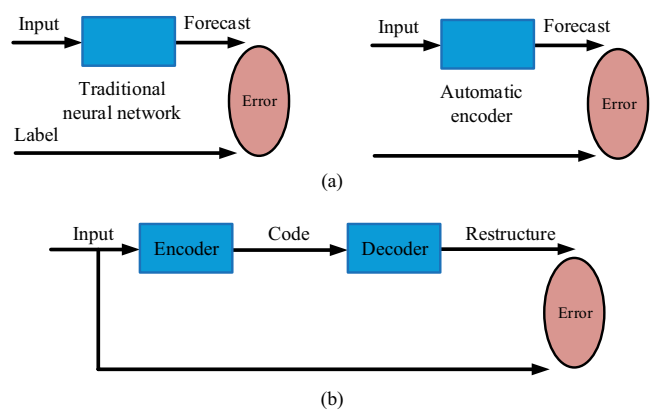Fig. 5. Multi-layer structure of deep learning model.

Fig. 6. Various operation mechanisms of sparse automatic coding.

where N represents the number of sampling points in Rayleigh wave phase velocity. From this, it can be observed that Vr_i^{obs} represents the phase velocity at the i sampling point, and Vr_i^{cal} represents the Rayleigh wave phase velocity at the i sampling point. Because of the inversion process, there are frequently some unclear components, which cause a variety of events to have less effect. The change trend of Rayleigh wave phase velocity caused by the change of density is small, that is, less than 10%. The change of longitudinal wave velocity can hardly affect the phase velocity of Rayleigh wave, and its influence is less than 3%. The change of P-wave velocity can hardly affect the Rayleigh wave phase velocity, and its influence is less than 3%. Based on this, the aforementioned inversion parameters may be specified, and a global optimization approach, namely the simulated annealing process, can be utilized for nonlinear solution. In the inversion process of the surface wave dispersion curve, it is required to input an initial guessing model, and set the disturbance model under the condition of fixed temperature. The perturbation when applying the simulated annealing algorithm is shown in Eq. (11).

$$Vs_{i+1}^j = Vs_i^j + a^j \left(V_2 - V_1 \right) \quad \text{and} \quad h_{i+1}^j = h_i^j + b^j \left(H_2 - H_1 \right) \qquad (11)$$

where a and b are the disturbance coefficients in the disturbance model, meeting the requirements of the probability distribution. Vs_i^j denotes the shear wave velocity of iteration i when it is located at layer j. In the same way, Vs_{i+1}^j denotes the shear wave velocity at the same layer number, but with the $i + 1$ iteration processing. h indicates the thickness of the layer, and its superscript and subscript have the same meaning as the shear wave velocity. Noteworthy is the fact that the values of V_1 and V_2 are related to Vr_{min}^{obs} and Vr_{max}^{obs}, respectively. The former is usually 1/2 of Vr_{min}^{obs}, and the latter is 3/2 of Vr_{max}^{obs}. Then the value range of shear wave velocity in layer j is determined as (V_1, V_2). The thickness of layer j is between H_1 and H_2. The value of H_1 is fixed as 0, and the value of H_2 is usually only half of the maximum Rayleigh wave length. Eq. (12) can improve the work efficiency in the disturbance model.

$$a, b = \text{sgn}\left(n - \frac{1}{2} \right) T \left[\left(1 + \frac{1}{T} \right)^{|2u-1|} - 1 \right] \qquad (12)$$

where the meaning of a and b remains the same, sgn( ) represents a step function, and T represents the temperature in the current environment. u satisfied $U(0,1)$ and evenly distributed. Because the model includes specific perturbation properties, such as a positive correlation between the search range and temperature, the perturbation effectiveness of Eq. (12) is greater. In summary, this perturbation technique has a greater perturbation efficiency and performance, as well as a quicker convergence speed. In addition, the updated calculation formula of P-wave velocity is shown below.

$$Vp = Vs \sqrt{\frac{2(1-\sigma)}{1-2\sigma}} \qquad (13)$$

Eq. (13) demonstrates that the P-wave velocity often needs to be determined according to Poisson's ratio σ on the basis of the obtained S-wave velocity, and the Poisson's ratio σ value is usually around 0.25.

4.3. Experimental design and analysis

The middle reaches of the Yangtze River's urban agglomeration's ecological imprint was estimated at the municipal level in this research. In terms of macro analysis, the urban agglomeration's total ecological demand may be studied to get the overall demand for its ecological environment, which comprises the carbon footprint, total ecological footprint, and urbanization rate. The specific analysis is shown in Fig. 7.

Fig. 7 demonstrates unequivocally that the entire the urban agglomeration's ecological imprint in the Yangtze River's middle reaches has grown year after year. The growth multiple and yearly growth rate have been extremely substantial, rising from around 76 million gha in 1998 to over 250 million gha in 2018. At the same time, during this time period, the pace of urbanization grew by nearly 1.37 times, while the rate of ecological footprint expansion remained much larger than the rate of urbanization. Overall, the pace of urbanization in the Yangtze River's middle reaches is about commensurate with the frequency of increase of the ecological footprint. During the initial period from 1998 to 2003, the pace of expansion of the urbanization process was substantially faster than the rate of increase of the ecological footprint.; from 2004 to 2012, the pace of increase in the ecological footprint steadily increased; It was not until 2013 that the pace of increase in the ecological footprint has tended to remain flat. During this time period, the changes of different types of ecological footprints are shown in Fig. 8.

Figs. 7 and 8 demonstrate that, in terms of different ecological footprint types, carbon footprint has occupied the largest proportion in the six ecological footprint types since 1998. The total ecological footprint is basically consistent with the growth trend of the total carbon footprint. It can be observed that carbon footprint is the biggest contributor to the increase in ecological footprint in the Yangtze River's middle reaches urban agglomeration. From the perspective of functional classification, it has been discovered as the productive footprint of organisms, the growth rate
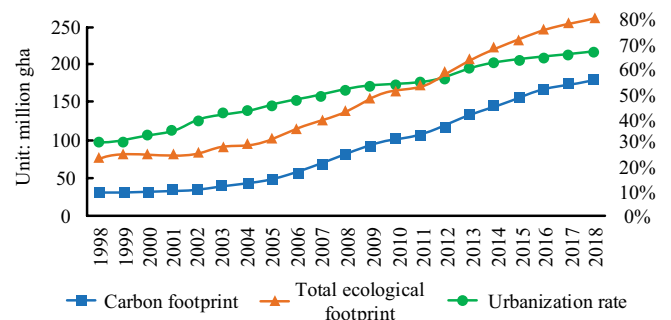

Fig. 7. Temporal changes of ecological footprint and carbon footprint of urban agglomeration in the middle reaches of the Yangtze River from 1998 to 2018.
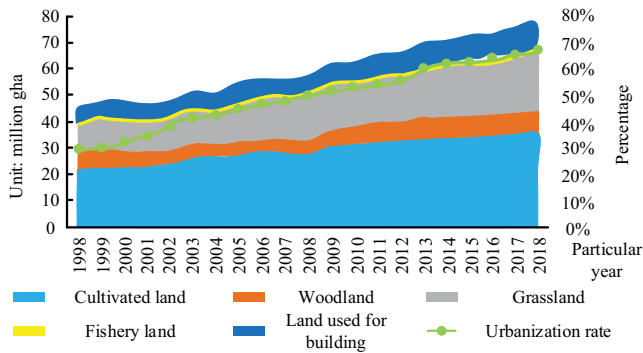
Fig. 8. Temporal variation of ecological footprint of different types of urban agglomerations in the middle reaches of the Yangtze River from 1998 to 2018.

of grassland footprint is extremely fast. The increase from around 10.15 million gha in 1998 to approximately 22.2 million gha in 2018 is substantial. The growth of fishery land and construction land should not be underestimated, with an increase of 98.4% and 99.6%, respectively. The explanation for this occurrence is that, as urbanization accelerates, per capita income and living standards of city dwellers continue to rise. Therefore, its demand for livestock meat and aquatic products is becoming more and more vigorous, and its requirements for living environment continue to increase. In a nutshell, the urban agglomeration along the middle reaches of the Yangtze River has become more urbanized during the last 20 y, and people's uncontrolled use of ecological resources has led to a significant rise in the overall ecological footprint, which has caused a noticeable impact on the ecological environment. Fig. 9 depicts the evolution of the per capita ecological footprint in this area over the same time period.

Fig. 9 shows that the ecological footprint per person's average yearly growth rate of the urban agglomeration in the Yangtze River's middle reaches was unusually high from 1998 to 2018, growing from 1.08 to 3.25 gha. From 1998 to 2004, the growth trend of per capita ecological footprint of urban enclave at the Yangtze River's middle reaches was relatively flat; From 2005 to 2009, the per capita ecological growth in the region showed a rapid upward trend; Except for 2013, the growth rate in all years from 2010 to 2018 was modest, indicating a tendency of steady development. On the other hand, in terms of different types of ecological footprint, even while all aspects of per capita ecological value have risen over time, the per capita carbon footprint continues to expand at a far faster rate. The per capita carbon footprint has grown from 0.43 gha to 2.26 gha. The footprint growth of per capita fishery land and per capita forest land is small. The per capita construction land has increased. In the past 20 y, Fig. 10 depicts a study of how the ecological footprint as a whole has changed over time.

Fig. 10 shows the changes of Theil index of the total ecological footprint, biological production footprint and carbon footprint of the Yangtze River's middle reaches urban agglomeration from 1998 to 2018. Theil index is a powerful tool for calculating and analyzing regional differences. Fig. 10 shows that the difference in total ecological footprint during the last 20 y is minimal, and the overall situation
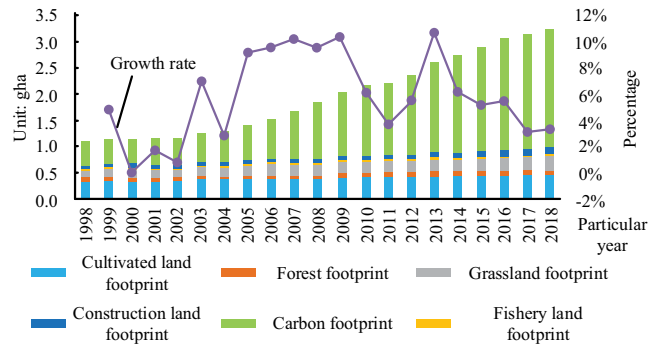

Fig. 9. Urban agglomerations in the middle reaches of the Yangtze River's ecological impact per person between 1998 and 2018.
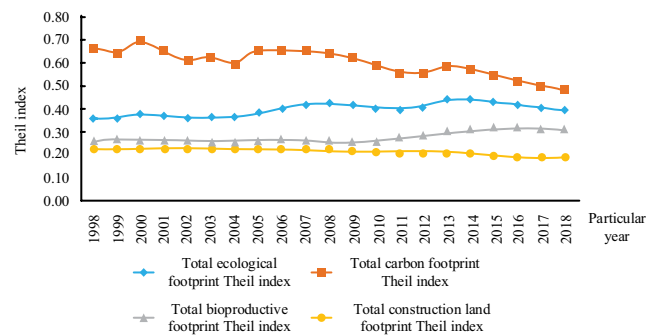

Fig. 10. C changes of total ecological footprint of urban agglomerations in the middle reaches of the Yangtze River from 1998 to 2018.

is changing and growing. Its Theil index rose continuously before 2013, and showed a downward trend of fluctuation after reaching the peak in that year. Theil index of total biological production footprint and total construction land footprint are both low. The only subtle difference is that around 2012, the former showed a slow upward trend of fluctuation, while the latter continued to decline. The carbon footprint is one of the most significant differences. The peak of its Theil index appeared in 2000, and then continued to decline; it dropped to the lowest point in 2018, only 0.485. In a nutshell, when the above four indicators are compared horizontally, the Thale index of carbon footprint is found to be the highest, indicating that carbon footprint is the primary reason for the difference in the entire ecological footprint of the Yangtze River's middle reaches urban agglomeration.

5. Conclusion

In recent years, various ecological warnings given to human beings by the continuously deteriorating ecological environment have made the ecological concept of sustainable development more and more respected all over the world. This study focuses on the various correlation factors of the ecological footprint, as well as its temporal and spatial evolution, and builds a deep learning model to analyze it to conduct detailed quantitative ecological footprint

investigation and explore the evolution trend of the ecological footprint. According to the study's results, from 1998 to 2018, the overall ecological footprint of the urban agglomeration in the Yangtze River's middle reaches rose year after year, including various types of ecological footprints, especially the most significant change in carbon footprint. The change of per capita ecological footprint presents a development trend of rapid growth to the peak and then slow growth. Furthermore, the Theil index of carbon footprint is the largest, and the difference varies greatly, with the lowest value of 0.485 appearing in 2018 and the maximum value of 0.698 appearing in 2000, respectively. Although this research has made significant progress in analyzing the chronological and geographical development of the three-dimensional ecological footprint of an urban agglomeration in the Yangtze River's middle reaches, there are still some gaps. For example, the investigation of urban agglomeration in the Yangtze River's middle reaches has not been detailed into a single city, and we believe that further progress may be done in the future.

Acknowledgments

References

[1]   N. Sillero, A. Márcia Barbosa, Common mistakes in ecological niche models, Int. J. Geogr. Inf. Sci., 35 (2021) 213–226.

[2]   J. Willard, X. Jia, S. Xu, M. Steinbach, V. Kumar, Integrating scientific knowledge with machine learning for engineering and environmental systems, ACM Comput. Surv., 55 (2022) 1–37, doi: 10.1145/3514228.

[3]   C. Li, Y. Zhang, S. Zhang, J. Wang, Applying the Super-EBM model and spatial Durbin model to examining total-factor ecological efficiency from a multi-dimensional perspective: evidence from China, Environ. Sci. Pollut. Res., 29 (2022) 2183–2202.

[4]   Q. Guan, Y. Yao, T. Ma, Y. Hong, Y. Bie, J. Lyu, Under the dome: a 3D urban texture model and its relationship with urban land surface temperature, Ann. Am. Assoc. Geogr., 112 (2022) 1369–1389.

[5]   K.D. Pearson, G. Nelson, M.F.J. Aronson, P. Bonnet, L. Brenskelle, C.C. Davis, E.G. Denny, E.R. Ellwood, H. Goëau, J. Mason Heberling, A. Joly, T. Lorieul, S.J. Mazer, E.K. Meineke, B.J. Stucky, P. Sweene, Machine learning using digitized herbarium specimens to advance phenological research, BioScience, 70 (2020) 610–620.

[6]   M. Pichler, V. Boreux, A.-M. Klein, M. Schleuning, F. Hartig, Machine learning algorithms to infer trait-matching and predict species interactions in ecological networks, Methods Ecol. Evol., 11 (2020) 281–293.

[7]   V. Hosu, H. Lin, T. Sziranyi, S. Saupe, KonIQ-10k: An ecologically valid database for deep learning of blind image quality assessment, IEEE Trans. Image Process., 29 (2020) 4041–4056.

[8]   F. Huang, J. Zhang, C. Zhou, Y. Wang, J. Huang, L. Zhu, A deep learning algorithm using a fully connected sparse autoencoder neural network for landslide susceptibility prediction, Landslides, 17 (2020) 217–229.

[9]   R. Barzegar, M.T. Aalami, J. Adamowski, Short-term water quality variable prediction using a hybrid CNN–LSTM deep learning model, Stochastic Environ. Res. Risk Assess., 34 (2020) 415–433.

[10] Z. Li, Y. Hu, Evaluation of the resource-environmental pressure based on the three-dimensional footprint family model: a case study on the Pearl River Delta in China, Environ. Dev. Sustainability, 24 (2022) 6788–6803.

[11] Y. Chen, H. Lu, J. Li, Y. Qiao, P. Yan, L. Ren, J. Xia, Fairness analysis and compensation strategy in the Triangle of Central China driven by water-carbon-ecological footprints, Environ. Sci. Pollut. Res., 28 (2021) 58502–58522.

[12] Y.-J. Lee, S.-Y. Lin, Vulnerability and ecological footprint: a comparison between urban Taipei and rural Yunlin, Taiwan, Environ. Sci. Pollut. Res., 27 (2020) 34624–34637.

[13] S. Wang, S. Chen, H. Zhang, Effect of income and energy efficiency on natural capital demand, Environ. Sci. Pollut. Res., 28 (2021) 45402–45413.

[14] Y. Achour, H.R. Pourghasemi, How do machine learning techniques help in increasing accuracy of landslide susceptibility maps?, Geosci. Front., 11 (2020) 871–883.

[15] S. Wang, L. Huang, X. Xu, J. Li, Spatio-temporal variations in ecological spaces and their ecological carrying status in China's mega-urban agglomerations, J. Geogr. Sci., 32 (2022) 1683–1704.

[16] H. Ke, S. Dai, H. Yu, Effect of green innovation efficiency on ecological footprint in 283 Chinese Cities from 2008 to 2018, Environ. Dev. Sustainability, 24 (2022) 2841–2860.

[17] A.A. Rafindadi, O. Usman, Toward sustainable electricity consumption in Brazil: the role of economic growth, globalization and ecological footprint using a nonlinear ARDL approach, J. Environ. Plann. Manage., 64 (2021) 905–929.

[18] M.T. Majeed, M. Mazhar, Reexamination of environmental Kuznets curve for ecological footprint: the role of biocapacity, human capital, and trade, Pak. J. Commer. Soc. Sci., 14 (2020) 202–254.

[19] A.A. Alola, T.S. Adebayo, S.T. Onifade, Examining the dynamics of ecological footprint in China with spectral Granger causality and quantile-on-quantile approaches, Int. J. Sustainable Dev. World Ecol., 29 (2022) 263–276.

[20] M. Usman, N. Hammar, Dynamic relationship between technological innovations, financial development, renewable energy, and ecological footprint: fresh insights based on the STIRPAT model for Asia Pacific Economic Cooperation countries, Environ. Sci. Pollut. Res., 28 (2021) 15519–15536.

[21] T. Chen, C. Song, C. Fan, J. Cheng, X. Duan, L. Wang, K. Liu, S. Deng, Y. Che, A comprehensive data set of physical and human-dimensional attributes for China's lake basins, Sci. Data, 9 (2022) 519, doi: 10.1038/s41597-022-01649-z.